

Article

Enhancing the Mechanical Properties of a 6061 Aluminum Alloy by Heat Treatment from the Perspective of Taguchi Design-of-Experiments

Isidro Guzmán-Flores ¹, Everardo Efrén Granda-Gutiérrez ^{2,*}, Celso Eduardo Cruz-González ³, Héctor Manuel Hernández-García ⁴, Juan Carlos Díaz-Guillén ⁵, Leonardo Flores-González ¹, Rolando Javier Praga-Alejo ¹ and Dora Irma Martínez-Delgado ⁶

¹ Facultad de Sistemas, Universidad Autónoma de Coahuila, Saltillo 25350, Mexico; isidroguzman@uadec.edu.mx (I.G.-F.); leonardo.flores@uadec.edu.mx (L.F.-G.); rolando_praga_alejo@uadec.edu.mx (R.J.P.-A.)

² Centro Universitario UAEM Atlacomulco, Universidad Autónoma del Estado de México, Toluca 50000, Mexico

³ Dirección de Ingeniería de Manufactura, Centro de Ingeniería y Desarrollo Industrial, Querétaro 76125, Mexico; ecruz@cidesi.edu.mx

⁴ InnovaBienestar de México, S.A.P.I. de C.V., Saltillo 25290, Mexico; hmanuelhdz@innovabienestar.mx

⁵ Consejo Nacional de Humanidades, Ciencias y Tecnologías—InnovaBienestar de México, Saltillo 25290, Mexico; jcarlos@innovabienestar.mx

⁶ Facultad de Ingeniería Mecánica y Eléctrica, Universidad Autónoma de Nuevo León, San Nicolás de los Garza 66455, Mexico; dora.martinezdl@uanl.edu.mx

* Correspondence: eegrandag@uaemex.mx



Citation: Guzmán-Flores, I.; Granda-Gutiérrez, E.E.;

Cruz-González, C.E.;

Hernández-García, H.M.;

Díaz-Guillén, J.C.; Flores-González, L.;

Praga-Alejo, R.J.; Martínez-Delgado,

D.I. Enhancing the Mechanical

Properties of a 6061 Aluminum Alloy

by Heat Treatment from the

Perspective of Taguchi

Design-of-Experiments. *Appl. Sci.*

2024, 14, 5407. [https://doi.org/](https://doi.org/10.3390/app14135407)

10.3390/app14135407

Academic Editor: Guian Qian

Received: 14 May 2024

Revised: 11 June 2024

Accepted: 17 June 2024

Published: 21 June 2024



Copyright: © 2024 by the authors. Licensee MDPI, Basel, Switzerland. This article is an open access article distributed under the terms and conditions of the Creative Commons Attribution (CC BY) license (<https://creativecommons.org/licenses/by/4.0/>).

Featured Application: This research on optimizing the heat treatment parameters of 6061-aluminum alloy could have practical applications in industries that rely on lightweight yet strong materials, such as the aerospace and automotive industries.

Abstract: This research investigates the heat treatment parameters of 6061-aluminum alloy to enhance its mechanical properties. The Taguchi design-of-experiments (DOE) method was employed to systematically examine the effects of solutionizing temperature, solutionizing time, aging temperature, and aging time on the tensile strength of the alloy. Mechanical testing suggested a major influence of solutionizing and aging temperatures on the ultimate tensile strength of the alloy. The samples subjected to a solutionizing temperature of 540 °C for 3 h, followed by aging at 170 °C for 18 h, exhibited the highest ultimate tensile strength (293.7 MPa). Conversely, the samples processed at the lowest levels of these parameters displayed the lowest ultimate tensile strength (193.7 MPa). Microstructural analysis confirmed the formation of equiaxed grains, strengthening precipitates, precipitate clusters, and β (Mg_2Si) precipitates alongside Fe-Al-Si dispersoids. Energy-dispersive X-ray spectroscopy (EDS) analysis detected the presence of elemental precursors of β phase (Al-Mg-Si) and dispersoid-forming elements (Al-Fe-Si). X-ray diffraction spectroscopy (XRD) analysis revealed the persistence of the β phase in the alloy, indicating its contribution to the improved mechanical properties, which are mainly obtained by aging precipitation phases. Fracture analysis showed a ductile fracture mechanism, and examining fractured samples supported the findings of enhanced tensile properties resulting from the adequate selection of heat treatment parameters. We employed ANOVA (analysis of variance) to analyze the DOE results, using a multiple regression model to express the ultimate tensile strength of the alloy in terms of the variables used in the design. This yielded an adjusted coefficient of determination of 89.75%, indicating a high level of explained variability in the test data for evaluating the model's predictive capacity.

Keywords: heat treatment processes; mechanical properties; 6061 aluminum alloy; Taguchi design of experiments; analysis of variance

1. Introduction

Structural aluminum alloys have gained increasing relevance in various sectors, and the automotive industry is one of its leading promoters. These alloys have found extensive applications; firstly, high-end vehicles have embraced their use for chassis and doors, but nowadays, other manufacturers have incorporated structural parts. The main advantage of aluminum alloys is weight reduction; when vehicles become lighter, they reduce energy consumption and improve fuel efficiency. Consequently, this is translated into cost savings for vehicle owners and significantly decreases CO₂ and other greenhouse gas emissions, positively impacting the environment [1–3].

One of the most-used aluminum alloys is the 6xxx series, a precipitation-hardening type. These alloys gain enhanced mechanical properties through heat treatment processes based on age hardening. 6xxx alloys are characterized by a main β hardening phase primarily composed of Mg₂Si, dispersed within the aluminum matrix. Various studies have determined the precipitation sequence of the β hardening phase by conducting solutionizing and aging heat treatments [4–7]. It is described as follows: supersaturated solid solution (SSSS) \rightarrow Si/Mg cluster \rightarrow Guinier–Preston (GP) zones \rightarrow β'' \rightarrow β' \rightarrow β . The β phase is the primary mechanism for strengthening these alloys.

Naronikar et al. [8] worked with 6061 alloys, implementing heat treatments by varying the temperature and treatment duration to improve the formability of sheets and plates. In their experimentation, they employed two types of heat treatments. First, a solutionizing treatment was conducted at 530 °C for 1 h, followed by water quenching. Then, an annealing heat treatment was performed at 415 °C for 2 h, followed by furnace cooling (according to the authors, this process is intended to avoid fractures during mechanical forming). After conducting an artificial aging process at 120 °C for 6 h, they reported 354 MPa as the alloy's ultimate tensile strength (UTS). The authors confirmed that heat treatment influences grain size and precipitate distribution, thereby improving the tensile mechanical properties of the alloy. In another example, Subba Rao et al. [9] performed a solutionizing treatment on a MoS₂-modified alloy at 520 °C for 1 h, followed by water quenching and aging at 180 °C for 12 h, obtaining a UTS = 246 MPa. These findings highlight the significance of carefully selecting heat treatment parameters to achieve the desired mechanical performance in aluminum alloys.

Using X-ray diffraction (XRD) and scanning electron microscopy (SEM), Aydia et al. [10] investigated an alloy after a solutionizing treatment at 580 °C for 5 h and aging at 185 °C for 6 h. The SEM analysis revealed the presence of structures such as Al-Fe-Si and the primary hardening phase (Mg₂Si), previously identified by Jacobs as the β phase [11]. Moreover, recent studies have determined that the precipitates in the 6xxx alloys are (a) precipitates of Mg₂Si, identified in optical microscopy as small, dark particles with an angular or globular shape, depending on the stage of aging; (b) precipitates of AlFeSi, which usually appear as elongated particles or plates, exhibiting an acicular (needle-like) or lamellar shape, and are typically larger than Mg₂Si precipitates; and (c) precipitates of AlMnSi, which are usually thicker and less numerous, appearing as spherical or irregularly elongated particles, and are generally larger than Mg₂Si precipitates but smaller than AlFeSi precipitates [12–14]. The main β phase distributed within the aluminum matrix favors tensile mechanical strength, achieving up to 206 MPa of UTS, but decreases corrosion resistance. Furthermore, fracture analysis of alloys subjected to solutionizing and aging heat treatments revealed a ductile fracture mechanism, typically characterized by dimples, as some researchers have demonstrated previously [15–17].

The mechanical properties of aluminum alloys are closely related to heat treatment parameters, as evidenced by the studies reviewed previously. In optimizing heat treatment conditions, employing specialized methodologies becomes helpful in effectively assessing the critical variables inherent in these processes. Among the techniques available, the Taguchi design of experiments (DOE) is a robust methodology devised by the Japanese engineer Genichi Taguchi. This approach simplifies processes and elevates product quality by highlighting the factors influencing performance and variability [18]. Its efficacy becomes

particularly important in scenarios necessitating meticulous tests and measurements to comprehend and predict mechanical properties, including tensile strength.

Several remarkable applications of Taguchi DOE in optimizing mechanical properties in materials have been documented. For instance, Leisk and Saigal [19] optimized the critical parameters of an aluminum heat treatment process to improve alumina/aluminum metal matrix composites, resulting in a notable increase in yield strength. Similarly, Yang et al. [20] utilized the Taguchi method to optimize heat treatment parameters for enhanced mechanical properties in a 2219 aluminum alloy produced via wire-arc additive manufacturing. Their findings emphasized the significant impact of solution temperature on alloy strength. Moreover, in the study undertaken by Afrasiabi et al. [21], the Taguchi DOE was employed to enhance the corrosion resistance of a 6061 aluminum alloy. By optimizing heat-treatment process parameters and investigating the effect of NaCl (sodium chloride) concentration, researchers successfully improved the alloy's resistance to corrosion. Another notable application was performed by Alphonse et al. [22], in which the Taguchi DOE was instrumental in identifying optimal heat-treatment parameters for a forged 2219 aluminum alloy, improving tensile strength and elongation percentage. These examples highlight the versatility and efficacy of the Taguchi DOE in optimizing mechanical properties across various materials and fabrication processes.

Our investigation was conducted to determine the phases present and the influence of the strengthening β phase on the tensile and hardness properties of a 6061-aluminum alloy. Solutionizing and artificial aging heat treatments were applied at various temperatures and for various durations based on a Taguchi experimental design. Characterization techniques such as XRD and SEM were employed to identify the phases and assess the tensile properties after the heat treatments. The Taguchi experimental design, through analysis of variance (ANOVA), facilitated the systematic selection of the heat treatment parameters, allowing for a comprehensive understanding of the relationship between the β phase and the mechanical properties of the alloy.

2. Materials and Methods

2.1. Analysis of Variance Foundations

Analysis of variance (ANOVA) is a powerful statistical tool that can be employed to assess the performance of a model in scrutinizing the influence of specific heat treatment parameters on a 6061 aluminum alloy. By analyzing the variance between different treatment groups, ANOVA allows us to determine whether variations in the alloy's mechanical properties, such as the ultimate tensile strength, can be attributed to the chosen parameters or if they occur by chance. It quantifies the significance of each parameter's impact, helping to identify the most influential factors shaping the alloy's properties. In this context, ANOVA is a critical tool for rigorously assessing and validating a model's effectiveness, providing information about heat treatment processes for enhanced material performance. We explain the theoretical basis of this technique in the following paragraphs.

ANOVA is a set of statistical models for studying the effect of one or more factors on the mean of a variable. To evaluate within-group variance compared to between-group variance, the "F₀ statistic" is used to determine whether the null hypothesis is accepted or rejected based on its value. Table 1 summarizes the analysis of variance to test the significance of a model, which starts from SS_{Mod} (the sum of squares, SS , of the model), as expressed in Equation (1) [23].

$$SS_{Mod} = \sum_{i=1}^n (\hat{y}_i - \bar{y})^2 \quad (1)$$

where n is the number of data samples, \hat{y}_i is the value predicted by the regression model, and \bar{y} is the mean of the process response.

Table 1. Analysis of variance parameters to assess the significance of the model. See Equations (1)–(9), where terms and literals are explained.

	SS	DF	MS	F ₀
Model	SS_{Mod}	k	MS_{Mod}	MS_{Mod}/MS_{Res}
Residual	SS_{Res}	$n - q$	MS_{Res}	-
Total	SS_{Tot}	$n - 1$	-	-

Similarly, the expression SS_{Tot} seen in (2) indicates the total sum of squares that measures the variability of y , being y_i the process response. On the other hand, SS_{Res} , exhibited in (3), is the sum of squares of the error that indicates the residual of the estimated model in explaining the response variable.

$$SS_{Tot} = \sum_{i=1}^n (y_i - \bar{y})^2 \tag{2}$$

$$SS_{Res} = \sum_{i=1}^n (y_i - \hat{y}_i)^2 \tag{3}$$

Furthermore, MS_{Mod} is defined as the mean squares (MS) of the model, and MS_{Res} as the mean squares of the residual, as can be seen in (4) and (5), respectively.

$$MS_{Mod} = \frac{SS_{Mod}}{k} \tag{4}$$

$$MS_{Res} = \frac{SS_{Res}}{n - q} \tag{5}$$

The degrees of freedom (DFs) are given by k as the number of input variables; n corresponds to the number of data; and q is expressed as $k + 1$.

Another relevant parameter is the coefficient of determination (R^2), which is a statistic commonly used to evaluate a hypothesis by determining the variability of the results of a model. The coefficient determines the ability of the model to replicate the results and the variation that can be explained. The equation for calculating the coefficient of determination is shown in (6).

$$R^2 = 1 - \frac{SS_{Res}}{SS_{Tot}} \tag{6}$$

Many regression users prefer to use an adjusted R^2_{adj} statistic, depicted in (7):

$$R^2_{adj} = 1 - \frac{SS_{Res}/(n - q)}{SS_{Tot}/(n - 1)} \tag{7}$$

$SS_{Res}/(n - q)$ is the residual mean square of error and $SS_{Tot}/(n - 1)$ is a constant. Consequently, R^2_{adj} increases only if a variable added to the model reduces the error mean square.

Finally, R -squared for prediction ($R^2_{prediction}$) is a statistic that tells us the percentage of variation in the outcome explained by the predictor variables. The equation that describes $R^2_{prediction}$ is given by (8), while the total sum of squares (SS_{Tot}) is given in (2).

$$R^2_{prediction} = 1 - \frac{PRESS}{SS_{Tot}} \tag{8}$$

PRESS measures how well the model will perform when predicting new data (i.e., data not used to fit the regression model). *PRESS* is calculated as follows (9):

$$PRESS = \sum_{i=1}^n \left(\frac{e_i}{1 - h_{ii}} \right)^2 \quad (9)$$

where e_i is the residuals ($y_i - \hat{y}_i$), \hat{y}_i is the value predicted by the regression model, and y_i is the process response. h_{ii} is the i -th diagonal element of the hat matrix H , given by $H = X'(X'X)^{-1}X$, X being the design matrix composed of the input variables.

2.2. Sample Preparation

For this investigation, a 6061 structural aluminum alloy was used, and its composition is shown in Table 2 as it was determined using a spark spectrometer. The aluminum alloy used was a commercial 6061-T6 alloy (as-received material). The designation of the T6 condition corresponds to a standardized classification system used to denote the heat treatment of an alloy (typically referring to a sheet or plate) aimed at altering its mechanical properties and hardness. In the case of alloy 6061, a range of designations from T1 to T38 exists. Specifically, T6 indicates that the alloy initially underwent a T4 treatment (a solutionizing heat treatment), followed by a subsequent precipitation hardening thermal treatment involving heating at 530 °C, succeeded by aging at 160 °C for 18 h, resulting in the designation T6 [24,25]. It is worth noting that we performed all tests with the alloy in the T6 condition from the supplier. The initial state characteristics are specified in the subsequent sections, presented in the results sections of the experimentation conducted in this research. For the heat treatment processes, samples with dimensions of 6.35 mm in thickness, 25 mm in width, and 70 mm in length were cut.

Table 2. Chemical composition of as-received 6061-T6 aluminum alloy.

Element (wt. %)								Other Not Specified (wt. %)	
Si	Fe	Cu	Mn	Mg	Cr	Zn	Ti	Individual	Total
0.75	0.62	0.38	0.14	1.10	0.33	0.25	0.15	<0.05	<0.15

To conduct the research, we proposed a design of experiment (DOE) using a Taguchi L27 (3^4) array [26] consisting of four factors: (A) solutionizing temperature, (B) aging temperature, (C) solutionizing time, and (D) aging time, and three levels: (1) low, (2) medium, and (3) high. The combination of levels and factors is presented in Table 3; in this table, each row represents a unique combination of factors and levels to be evaluated. For example, row 1 corresponds to testing factor A at level 1, factor B at level 1, factor C at level 1, and factor D at level 1. Similarly, row 2 corresponds to testing factor A at level 1, factor B at level 2, factor C at level 2, factor D at level 2, and so on. The selection of solutionizing and aging temperatures and duration was based on existing literature, mainly the references analyzed in the Introduction [8–10], where similar values are reported, but also relevant international standards and guidelines [24,27]. Also, we selected the temperature and time intervals that we found to be useful in heat treatments that we have used in welding processes [14,28,29]. The three levels for the solutionizing temperature were 520, 530, and 540 °C; the levels for the solutionizing time were 3, 4, and 5 h; for aging temperature, we proposed 150, 160, and 170 °C; and for the aging time, we used 12, 18, and 24 h. A muffle furnace was utilized to perform solutionizing and aging heat-treatments based on the combinations described in Table 3.

Table 3. Taguchi L27 (3^4) orthogonal array for the 4 factor–3 level heat-treatment process.

Run	Level Combination	Factor A Sol. Temp. ($^{\circ}$ C)	Factor B Sol. Time (h)	Factor C Aging Temp. ($^{\circ}$ C)	Factor D Aging Time (h)
1	1-1-1-1	520	3	150	12
2	1-2-2-2	520	4	160	18
3	1-3-3-3	520	5	170	24
4	2-1-2-3	530	3	160	24
5	2-2-3-1	530	4	170	12
6	2-3-1-2	530	5	150	18
7	3-1-3-2	540	3	170	18
8	3-2-1-3	540	4	150	24
9	3-3-2-1	540	5	160	12

In the context of experimental design, selecting factors and levels is crucial in determining the efficiency and effectiveness of the study. When designing our experiment, we carefully identified known or hypothesized variables to influence the response variable, which, in our case, is the ultimate tensile strength (UTS) of the alloy. These factors were chosen based on a literature review, as mentioned in the precedent paragraph, and our understanding of the material properties and heat-treatment processes involved. Each selected factor has a potentially significant impact on the response.

Furthermore, the decision to include four factors and three levels each was made carefully considering the capabilities of the Taguchi DOE methodology [18]. The L27 Taguchi design allows for the construction of an orthogonal matrix with unique combinations of factors and levels. This orthogonal matrix ensures that each factor level combination is represented evenly, thereby providing a statistically robust representation of the experimental set. By utilizing this orthogonal array, we can efficiently explore the parameter space with limited experimental runs. This minimizes the resources and time required for experimentation and maximizes the information obtained from each experiment. Using the L27 (3^4) array, nine unique experimental runs can be conducted, each corresponding to one row in Table 3. Each experiment was conducted thrice to ensure proper replicability; consequently, we performed 27 experiments. The data collected from these runs can then be used to analyze the effects of the factors and determine the optimal combination of factors and levels for the desired outcome.

2.3. Experimental Analysis

After the heat-treatment, tensile tests were performed, based on the ASTM E-8 standard [30], on plate specimens 6.35 mm in thickness, with a reduced section 12.5 mm in width and 63 mm in length, and 50 mm in gauge length (to attach the extensometer). Testing speed has a strong influence on measured mechanical properties (annex X1 in [30]); then, assuring the limits stated in this standard guarantees good repeatability and confidence in testing results (Section 9 in [30]). The standard limits of the testing speed to calculate tensile and yield properties shall be between 1.15 and 11.5 MPa/s and a factor of 0.05 and 0.5 min^{-1} of the test zone length to calculate the testing speed limits. Thus, given the test zone length of 63 mm, the speed of the test ranges from 3.5 to 35 mm/min (Section 7.6.4 in [30]). Consequently, we used a tensile rate of 10 mm/min and a yield speed of 8 MPa/s to determine the ultimate tensile strength (UTS), Young's modulus, yield strength (0.2% offset), and final elongation.

Hardness measurements were performed with a 250 gf load with a microhardness tester. Metallography was conducted following the ASTM E3 standard [31]. An optical microscope was employed for microstructure analysis, and images were analyzed using Nikon NIS Elements D software version DS-03. Fractography and phase identification were performed using a scanning electron microscope (SEM) equipped with an energy-dispersive X-ray spectroscopy (EDS) sensor. Phase identification was accomplished using an Empyrean Panalytical X-ray diffractometer. The analyses were conducted in microd-

iffraction mode on a 1 mm × 1 mm area where High Score Plus 5.0 software and PDF+ database were utilized for phase analysis. Each sample was subjected to a 0.0016° step size with a counting time of 87.92 s. XRD analysis was performed from 30° to 80° (2θ) using Cu_{kα} radiation (45 kV, 40 mA).

3. Results

3.1. Tensile Strength Evaluation

Table 4 presents the tensile test results (average of three repetitions) after the experimental series from the combination of parameters exhibited in Table 3 was conducted (DOE). The analysis begins by explaining and interpreting the tensile test results because they serve as the starting point for the microstructural analysis of the samples and the further investigation of fracture behavior. Also, the ultimate tensile strength is an indicator or reference for the study of the Taguchi DOE and ANOVA.

Table 4. Tensile test results after executing the DOE. Values in parenthesis are the standard deviation of three repetitions.

Run	Level Combination	UTS (MPa)	Young Modulus (GPa)	Yield Strength (MPa)	Signal-to-Noise Ratio (dB)
1	1-1-1-1	193.7 (8.7)	57.20 (2.46)	157.7 (32.7)	45.723
2	1-2-2-2	219.0 (3.5)	45.00 (2.33)	176.0 (27.2)	46.807
3	1-3-3-3	281.7 (5.0)	52.47 (4.91)	134.7 (19.4)	48.992
4	2-1-2-3	246.3 (3.1)	51.37 (4.30)	187.0 (21.1)	47.829
5	2-2-3-1	270.0 (0.0)	61.07 (3.29)	191.3 (58.0)	48.627
6	2-3-1-2	223.3 (3.2)	55.23 (3.97)	138.0 (5.0)	46.977
7	3-1-3-2	293.7 (1.5)	57.87 (2.87)	180.7 (28.0)	49.357
8	3-2-1-3	252.7 (3.1)	58.33 (2.87)	217.0 (44.2)	48.050
9	3-3-2-1	248.7 (4.7)	56.07 (0.90)	221.3 (10.8)	47.909

As a reference, we measured the tensile strength of the as-received alloy, which was found to be 274 MPa with a standard deviation (SD) of 10 MPa. Although a mechanical strength of 290–310 MPa is often mentioned in the literature as a typical value for 6061-T6 alloy, the ASTM B209 standard [32] specifies a minimum UTS value of 42 ksi (approximately equivalent to 289 MPa). Then, our measured UTS of 274 MPa (SD = 10 MPa) for the as-received material is, to some extent, slightly below this minimum specification.

However, it is important to note that we purchased the commercial plate from a local supplier and assumed inherent variations as accounted for in the ASTM E8 standard, particularly Table X1.1 in [30], where a repeatability and reproducibility (R&R) value of 12.1 MPa is reported, indicating variability due to sampling. Given this context, our measurement of 274 MPa falls within the acceptable range when considering the reported tolerance value and our measurement precision.

Furthermore, the UTS of 293.7 MPa (SD = 1.5 MPa) obtained from our best condition after the heat treatment study indeed shows an improvement compared to the original strength of the as-received alloy. This result emphasizes the main point of our research: the significant influence of solutionizing and aging parameters on the mechanical properties of the alloy, from a Taguchi DOE perspective.

Thus, UTS was chosen as the primary output response, and a criterion of the larger-the-better approach was selected. The signal-to-noise (S/N) ratio for each run is calculated as the negative logarithm of the reciprocal of the squared output value. The average S/N ratio for a particular factor level combination is then determined as follows:

$$\frac{S}{N} = -10 \log_{10} \left(\frac{1}{m} \sum_{i=1}^m \frac{1}{y_i^2} \right) \quad (10)$$

where m is the number of replicates, 3 for our L27 (3^4) design; and y_i is the response variable value for the i -th replicate. Once the S/N ratios for each combination of factor levels are calculated, they can be compared and analyzed to determine the optimal factor level settings that maximize the S/N ratio for the specific objective.

The samples that exhibited the best mechanical tensile properties among the tested samples were those in the 7th run (see Table 4); also, this run showed the maximum S/N ratio of 49.357 dB, according to the criterion of “the larger, the better”. These samples were processed at a solutionizing temperature of 540 °C or 3 h, followed by aging at 170 °C for 18 h, resulting in an average ultimate tensile strength of 293.7 MPa. In contrast, samples from the 1st run exhibited the lowest mechanical properties; they were subjected to a solutionizing temperature of 520 °C for 3 h and aging at a temperature of 150 °C for 12 h, yielding a significantly lower UTS, of only 193.7 MPa. The sample comparison demonstrates the considerable influence of the solutionizing and aging parameters on the resulting mechanical properties, as can be inferred from Table 4. Stress vs. strain curves for selected samples are exhibited in Figure 1 (only the 3 best and the worst samples were plotted); please note that numerical values of UTS for each individual combination of factors are exhibited in Table 4.

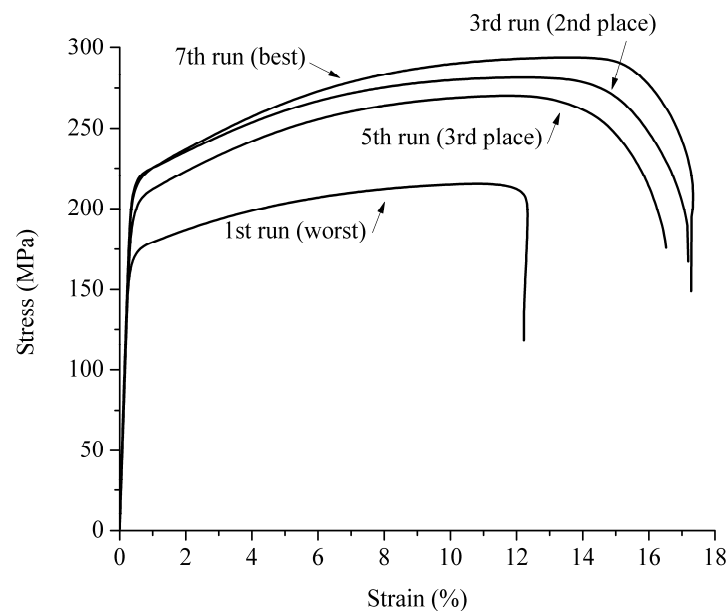


Figure 1. Stress–strain curves for selected samples.

3.2. Analysis of Variance and the Fit Result of the Model

Once UTS was determined to be the primary output parameter, the models’ behavior and their variables were analyzed by constructing an ANOVA table. We proposed a design of experiment (DOE) using a Taguchi L27 (3^4) array (see the experimental parameters of DOE in Table 3 and the results of the experiments in Table 4), using the residuals and the total sum of squares to calculate the source of variation of the models (as specified in Table 1).

Table 5 shows the ANOVA performed for the regression model, considering all 27 experiments that were realized based on the combinations of levels and factors previously specified in Table 3. The model is representative by having a p -value < 0.05 ; i.e., the model adequately represents the variability that occurs in the process. This comprehensive analysis allows us to assess the significance and contribution of each factor and its interactions across the entire experimental matrix.

Table 5. Summary of the ANOVA based on the 27 experiments performed for this work. Observe that the aging temperature (in bold) is not statistically significant in the UTS value.

Source	SS	DF	MS	F ₀	p-Value
Regression Model	23,078.8	4	5769.7	75.20	≈0
Solutionizing temperature	5017.6	1	5017.6	65.39	≈0
Aging temperature	214.3	1	214.3	2.79	0.109
Solutionizing time	15,500.5	1	15,500.5	202.02	≈0
Aging time	2346.4	1	2346.4	30.58	≈0
Residual	1688	22	76.7		
Total	24,766.9	26			

The probability p -value is an approach for making decisions in hypothesis tests. One way to report the results of a hypothesis test is to state that the null hypothesis (usually denoted H_0) was or was not rejected at a specified α -value or significance level; this α -value is typically 0.05. The p -value is the probability that the test statistic will take on a value that is at least as extreme as the observed value of the statistic when the null hypothesis H_0 is true [33]. A p -value conveys a lot of information about the weight of evidence against H_0 so that a decision-maker can draw conclusions at any significance level. Thus, the p -value is the smallest level of significance that would lead to the rejection of the null hypothesis H_0 with the given data. It is customary to call the test statistic (and the data) significant when the null hypothesis H_0 is rejected; therefore, we may consider the p -value the smallest level at which the data are significant. Once the p -value is known, the decision maker can determine how significant the data are without the data analyst formally imposing a preselected significance level (in this case, $\alpha = 0.05$). Please note that a p -value of approximately zero implies that it is much lower than the significance level (see Table 5).

The ANOVA for the regression model using the Taguchi L27 (3^4) array method can be seen in Table 5. This adequately represents what happens in the process by having a $p < 0.05$, and the calculated F is higher than the F distribution in $1 - \alpha = P(F \leq f_\alpha, 4, 12)$ with $\alpha = 0.05$, indicating that the model rejects the null hypothesis and concludes that the ultimate tensile strength of the alloy is linearly related to four factors: (A) solutionizing temperature, (B) aging temperature, (C) solutionizing time, and (D) aging time. Additionally, we intend to identify which variables have a greater weight in the model and process, where it is observed that the tensile strength model is less affected by the variable aging temperature with a value $p = 0.109$ ($p > 0.05$) and a calculated F of 2.79, noting that this has a lower weight in the model. Therefore, this variable does not have statistical significance to the ultimate tensile strength value when compared with the p -value of the other parameters. This observation is supported by the p -value reported for the aging temperature variable, which was found to be $p = 0.109$. In contrast, the p -values for the other variables (solutionizing temperature, solutionizing time, and aging time) were all below the significance threshold of 0.05, indicating their statistical significance with respect to the response variable.

The linear regression model was fitted using the data collected by the Taguchi array method from the 27 performed experiments (see Table 4). As a result of this process, the resultant model is shown in Equation (11):

$$\hat{y} = \beta_0 + \beta_1 x_1 + \beta_2 x_2 + \beta_3 x_3 + \beta_4 x_4 \quad (11)$$

where the intercept (β_0) and slope ($\beta_1, \beta_2, \beta_3, \beta_4$) of the line are called regression coefficients, and x_1, x_2, x_3, x_4 are the factors (or regressors) involved in the DOE (solutionizing temperature, aging temperature, solutionizing time, and aging time, respectively) affecting the predicted output (\hat{y}), i.e., the UTS value.

In that case, the ultimate tensile strength (UTS) can be expressed as (12):

$$\text{UTS} = -1155 + 1.670 * \text{solutionizing temp.} + 3.45 * \text{aging temp.} + 2.935 * \text{solutionizing time} + 1.903 * \text{aging time} \quad (12)$$

It is reasonable to assume that the mean of the random variable Y is related to X by Equation (11) as a straight-line relationship, and its solution is given by Equation (12). While the mean of Y is a linear function of X , the actual observed value (y) does not fall exactly on a straight line. The appropriate way to generalize this to a probabilistic linear model is to assume that the expected value of Y is a linear function of X , but that for a fixed value of X the actual value of Y is determined by the mean value function (the regression linear model) [34]. This is a multiple linear regression model because it has various independent variables or regressors. Sometimes, a model like this will arise from a theoretical relationship. At other times, we will have no theoretical knowledge of the relationship between X and y .

Thus, the regression model in (11) is a line of mean values; that is, the height of the regression line at any value of x is just the expected value of Y for that x . β_0 (in this case $\beta_0 = -1155$) is the value of the predicted variable when all regressors are equal to zero, while $\beta_1, \beta_2, \beta_3, \beta_4$ can be interpreted as the change in the mean of Y for a unit change in x . Furthermore, the variability of Y at a particular value of x is determined by the error variance (σ^2). This implies that there is a distribution of Y – values at each x and that the variance of this distribution is the same at each x .

In this case, $Y = \text{UTS}$, the intercept $\beta_0 = -1155$, and the slopes are $\beta_1 = 1.670, \beta_2 = 3.45, \beta_3 = 2.935, \beta_4 = 1.903$. The input variables are in X as follows: solutionizing temperature = x_1 , aging temperature = x_2 , solutionizing time = x_3 , and aging time = x_4 (see Equation (12)). Consequently, the regression model shows that the relationship between Y and the input variables are at a level x . Then this fitted regression equation or model can be used in prediction of future observations of Y or for estimating the mean response at a particular level of x .

3.3. Hardness Evaluation

After the heat-treatment process, the hardness of the samples was also assessed. The investigation revealed that fluctuations in hardness primarily depend on the solutionizing temperature. The summarized results are presented in Figure 2, representing the hardness of all samples treated at a specific solutionizing temperature; it provides valuable insights into the microhardness's behavior.

Previous authors [10,35] have determined that hardness depends on the presence of alloying elements such as Mg and Si, which form intermetallic phases in the presence of Fe, among other elements, as well as the time and temperature of the aging process. With a solutionizing temperature of 540 °C for 3 h, followed by artificial aging at a temperature of 170 °C for 18 h, hardness of up to 98 HV (SD = 2 HV) was achieved. At these solutionizing temperatures, a more significant quantity of alloying elements can be retained as a solid solution, allowing for the precipitation of alloying elements during artificial aging, which forms strengthening phases.

The hardness of an alloy is primarily attributed to the presence of GP zones and strengthening phases, as reported previously [36–39]. Notably, at a temperature of 540 °C, the precipitation of Mg_2Si phases and GP zones is favored; then, microhardness values of up to 98 HV (SD = 2 HV) were obtained for these samples. In contrast, the lowest microhardness was observed for a solutionizing temperature of 520 °C.

The initial microhardness of the as-received sample was measured as 101 HV (SD = 4.5 HV), but it is worth noting that a slightly increased hardness does not necessarily enhance the maximum mechanical strength [38,39].

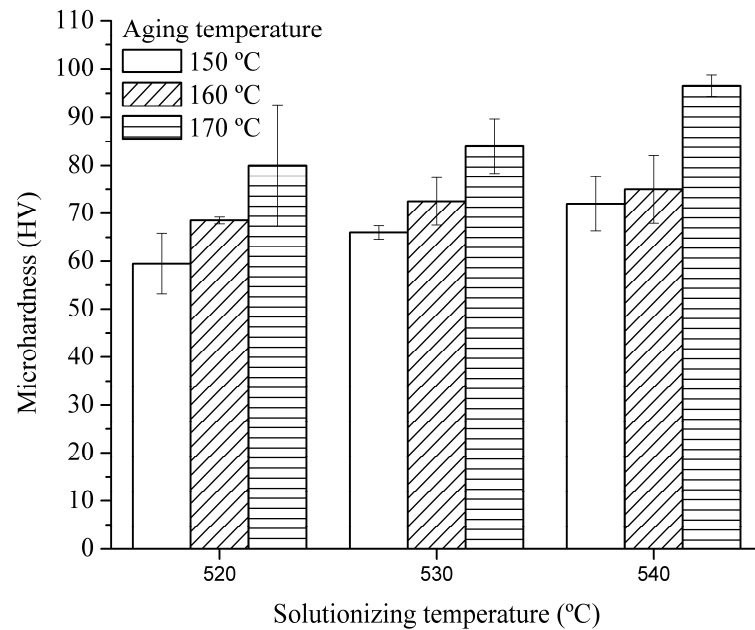


Figure 2. The average microhardness of heat-treated samples as a function of aging and solutionizing temperatures. Error bars are the standard deviation.

Although the change from an average of 101 HV (SD = 4.5 HV) for the as-received material to 98 HV (SD = 2 HV) is not significant, it is important to understand that a slight decrease in hardness does not necessarily correlate with a reduction in mechanical strength. As described by various authors [15–17], the β phases (Mg_2Si) present in the as-received material become more voluminous and well-distributed after artificial aging. During the aging process, the β phases precipitate and re-distribute within the aluminum matrix, a phenomenon we confirmed using X-ray diffraction (see Section 3.5).

According to Demir and Gündüz [40], increasing the aging time enhances re-precipitation, resulting in increased hardness due to the impeded mobility of dislocations caused by precipitate formation. However, prolonged aging can lead to the coarsening of precipitates, reducing their effectiveness as obstacles to dislocation movement and, consequently, decreasing hardness. This balance between precipitate distribution and size significantly influences the material's mechanical properties (see Section 3.4).

In our case, the observed increase in UTS in the 7th run sample (293.7 MPa) compared to the as-received material (274 MPa) can be attributed to the better re-distribution and size of the precipitates achieved through our specific heat-treatment regimen. The artificial aging process used in our experiments led to a favorable precipitate structure that enhanced tensile strength without a corresponding increase in hardness. The reduced hardness (98 HV) indicates a more refined precipitate distribution, which can improve the tensile strength by effectively blocking dislocation motion, thereby increasing UTS.

While the hardness change was minimal, the substantial increase in UTS reflects the successful optimization of the precipitate structure through our heat-treatment process, leading to improved mechanical performance of the alloy.

3.4. Microstructural Analysis

After the heat-treatment, the samples were removed from the furnace, and cross-sections were prepared to analyze their microstructure utilizing SEM. The microstructural results presented here correspond to selected samples from the tensile tests shown in Table 4. Figure 3 depicts the microstructure of the as-received alloy material. Equiaxed grains, characteristic of the 6061-T6 alloy, can be observed in Figure 3a; additionally, Figure 3b shows the presence of Al-Fe-Si dispersoids.

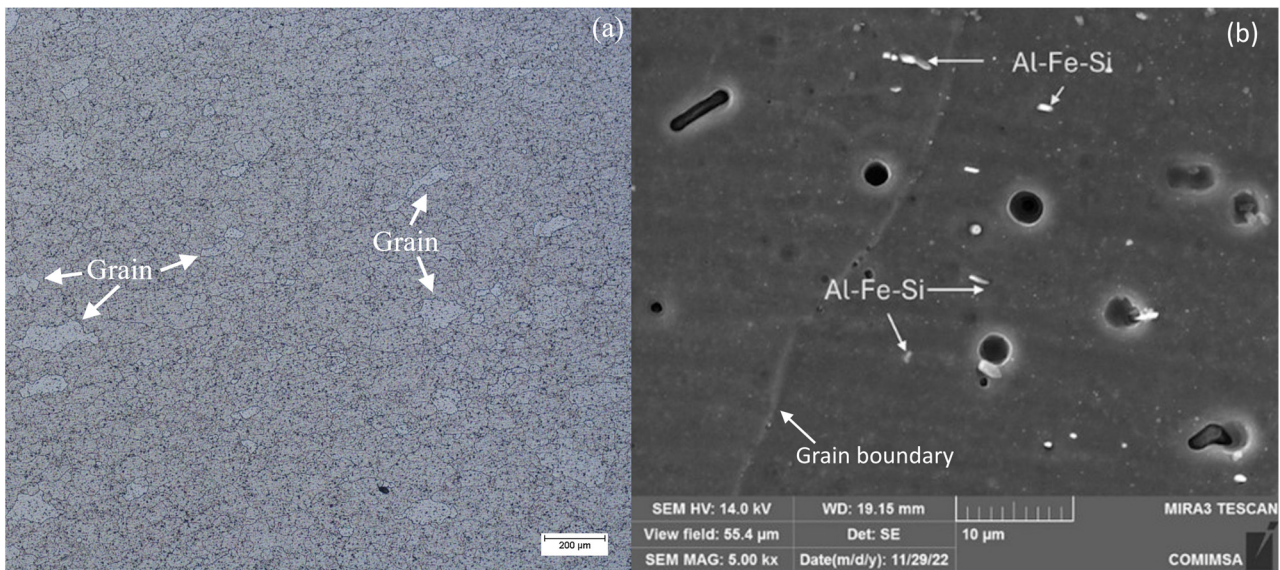


Figure 3. (a) Micrographs of the as-received material exhibiting the grain distribution in the Al matrix and (b) as-received material exhibiting Mg_2Al (β phase) characterized by plates and needle morphologies.

As-received material was also analyzed by EDS, and its spectrum is exhibited in Figure 4. It is worth mentioning that the sample exhibited some particles of Al-Fe-Si, as observed previously in Figure 3. However, EDS analysis revealed that Mg is also present in the metallic matrix, as well as traces of Si. The latter suggested the presence of other phases, mainly the β phase, as would be further confirmed by XRD (see Section 3.5). Small traces of Fe were also detected by the equipment.

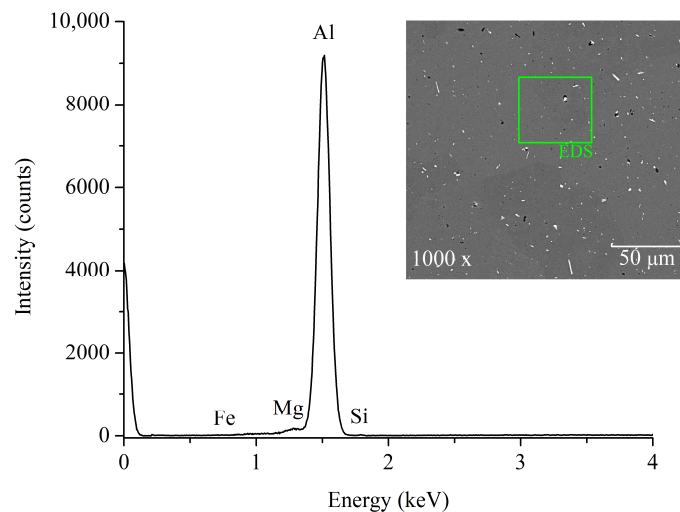


Figure 4. EDS spectrum of an area of approximately $50 \times 50 \mu m$ in the as-received samples exhibiting the presence of aluminum and magnesium.

Figure 5a shows the micrograph of a selected sample from the 7th run of the DOE, where equiaxed grains are visible. Also, Figure 5b exhibits strengthening precipitates, precipitate clusters, and β precipitates alongside Fe-Al-Si dispersoids [12,14].

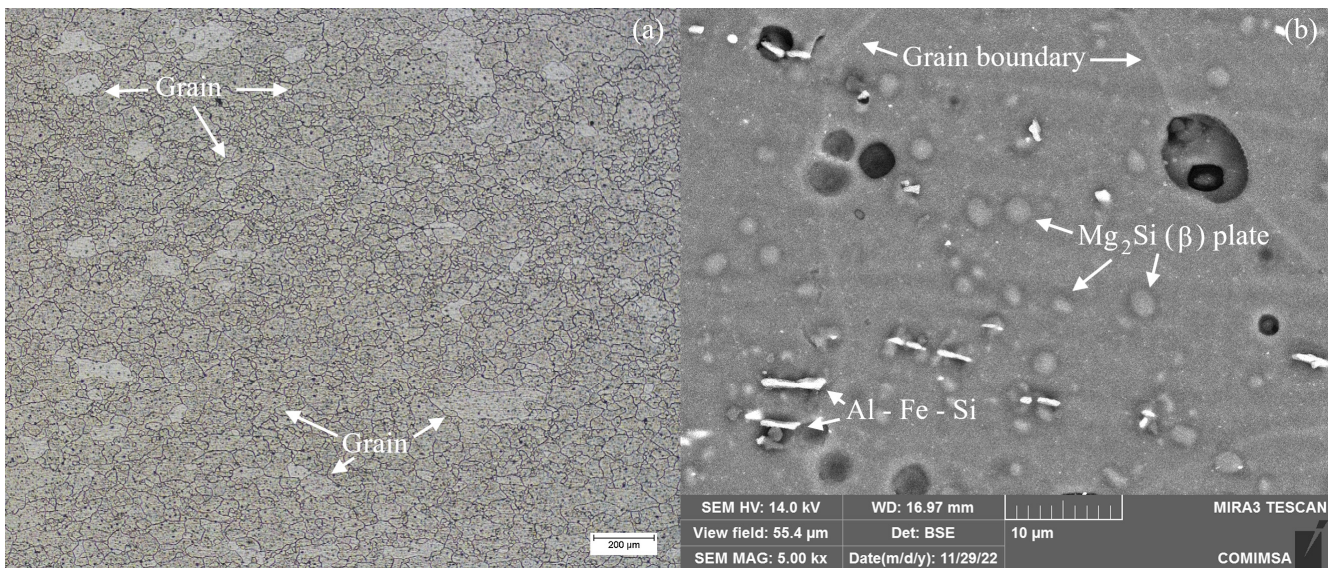


Figure 5. (a) Equiaxed grains on the heat-treated surface of a representative sample from the 7th run of the DOE and (b) precipitates in the Al matrix on the surface of the same sample.

The presence of β phases and dispersoids in the sample with the best mechanical condition (7th run) was confirmed using EDS in Figure 6. The representation of EDS spectra was performed in an energy range from 0 to 4 keV to highlight traces of Mg (at 1.2 keV), Si (1.75 keV), and Fe (0.65 keV) precursor elements. These elements exhibit much lower relative intensities compared to the characteristic peak of Al, which is at 1.5 keV. Although the original test was conducted in a range of 0 to 7.5 keV, no traces of Mg, Si, or Fe were identified at other energy values, leading to the decision to more clearly display the peaks that are most visible near the characteristic peak of Al.

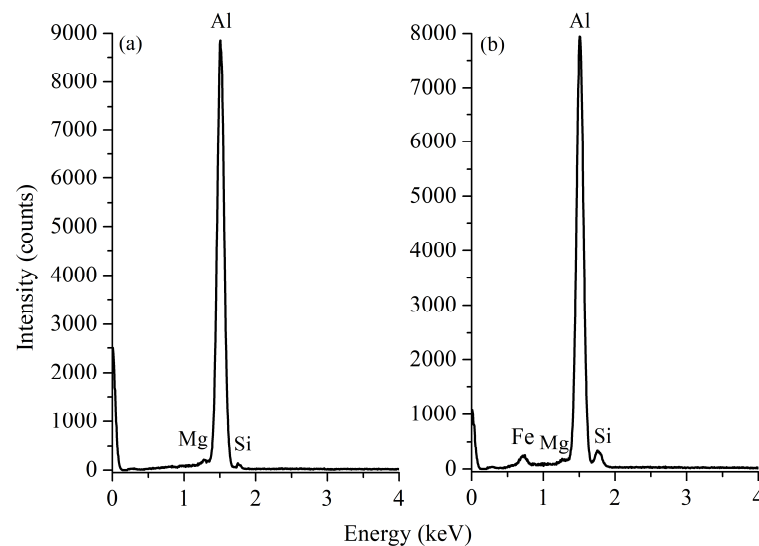


Figure 6. EDS spectrum exhibiting (a) elements precursors of β phase (Al-Mg-Si) and (b) dispersoid-forming elements (Al-Fe-Si).

3.5. XRD Phase Identification

We utilized XRD analysis to identify the β phase. The identification of the strengthening phase presents challenges because the predominant peaks of aluminum from the aluminum matrix complicate intensity measurements, leading to potential confusion between the crystallographic planes of hexagonal aluminum corresponding to the β phase

and the FCC structure of the aluminum matrix. However, it is still possible to distinguish the β phase with careful analysis, as explained in the following paragraphs.

Figure 7a presents the XRD pattern of the as-received sample; the highest peak corresponds to aluminum with (200) orientation. By zooming in on the spectrum in Figure 7b, the presence of the β phase (Mg_2Si) with (220) orientation becomes more evident. Traces of the aluminum matrix with orientations (111) and (311) are also observed [41].

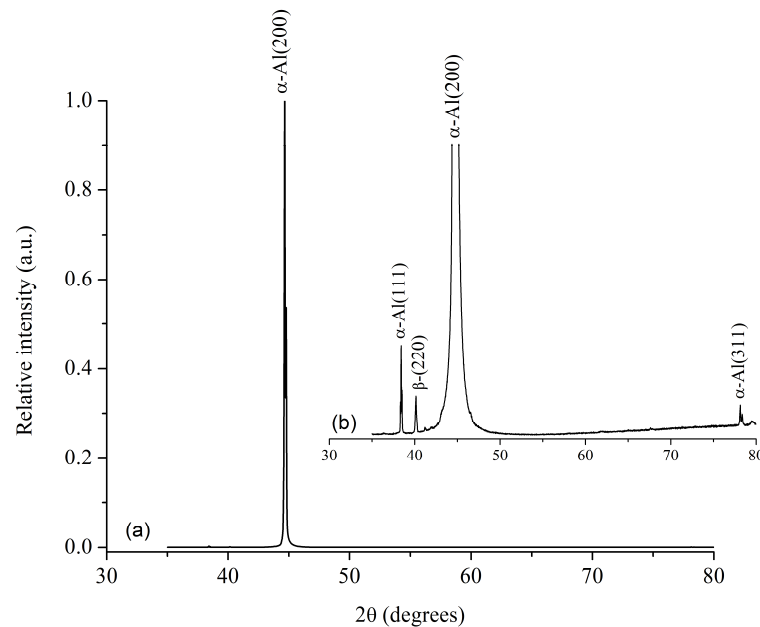


Figure 7. (a) XRD spectra for 6061 aluminum alloy (as-received) at full scale; (b) amplification of the trace peaks.

Figure 8 shows the XRD spectrum corresponding to the sample that exhibited the lowest mechanical properties (1st run), in which the presence of the β phase with orientation (220) is observed. The presence of aluminum peaks having the orientations (111), (220), and (311) is noticeable with greater relative intensity compared to the as-received sample.

Figure 9 presents the XRD pattern of a representative sample from the 7th run, subjected to a solubilization temperature of 540 °C for 3 h and aging at 170 °C for 18 h. It can be confirmed that the thermal treatment has induced recrystallization in the aluminum matrix. This is evident from the altered orientation of the aluminum diffraction peak initially observed at (200) in Figure 7. Furthermore, Figure 9 demonstrates a change in the relative intensity of other peaks, indicating the presence of the β phase in the alloy. According to the literature, the morphology of the β phase is typically observed in the form of plates or needles [11], as previously depicted in Figure 5, which corroborates the XRD findings. It is important to note that increasing the solution time can result in the dissolution of a more significant amount of the β strengthening phase, leading to increased hardening after the solution treatment [42]. Therefore, traces of the beta phase can be observed in Figures 7–9.

The recrystallization of the aluminum matrix after the thermal treatment is a significant phenomenon in alloy processing. Recrystallization refers to forming new grains with a lower dislocation density and improved structural stability. In this case, the observed shift in the diffraction peak of aluminum (200) suggests a realignment of crystallographic planes, indicating the occurrence of recrystallization. The recrystallization process promotes the development of a more uniform and fine-grained microstructure, which can contribute to enhanced mechanical properties, such as increased strength and improved formability.

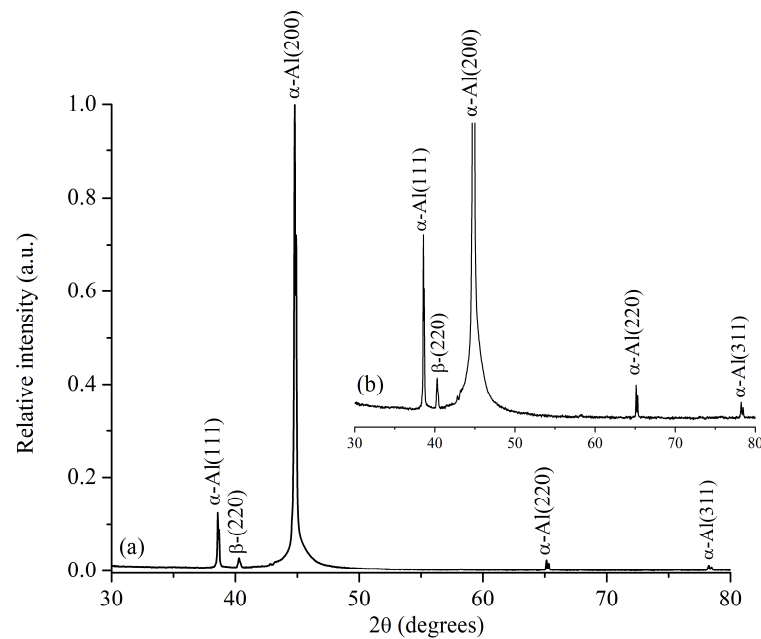


Figure 8. (a) XRD spectra for the heat-treated 6061 aluminum alloy at full scale (1st run, worst case); (b) amplification of the trace peaks.

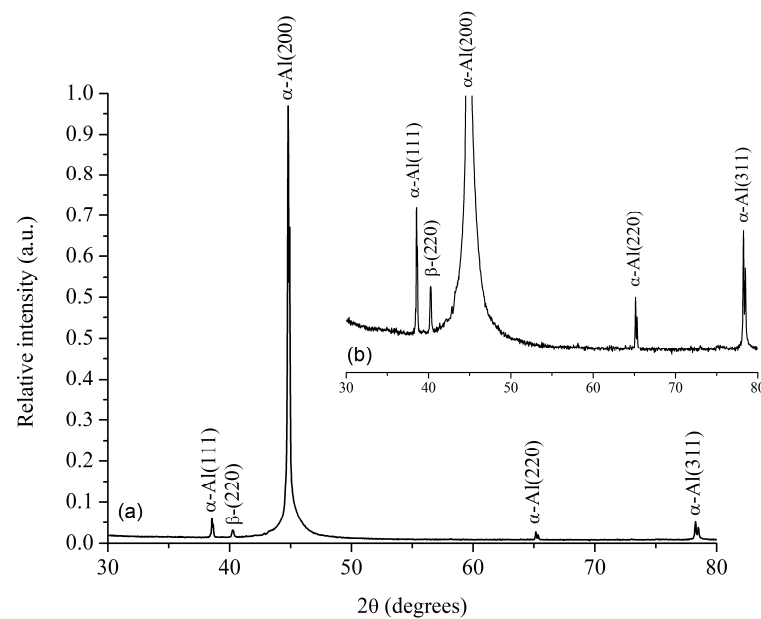


Figure 9. (a) XRD spectra for the heat-treated 6061 aluminum alloy at full scale (7th run, best case); (b) amplification of the trace peaks.

3.6. Fracture Mechanisms

An interesting aspect of this study is the evaluation of the fracture mechanisms in the different experimental samples. First, we present the fractography shown in Figure 10, which corresponds to the sample from run 1, which exhibited the lowest UTS among all the samples. The fractographic analysis reveals the presence of microvoids, characteristic of ductile fracture. However, we also observe traces of cleavage, indicative of brittle fracture. Therefore, this sample exhibited a mixed fracture mechanism, combining both ductile and brittle features [43,44].

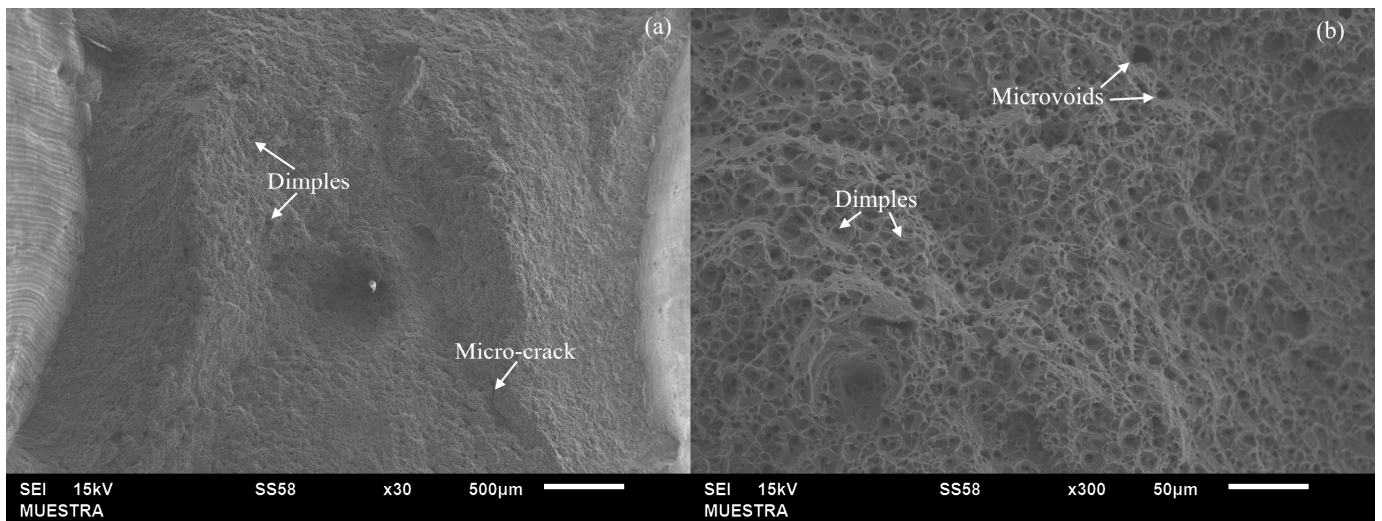


Figure 10. (a) Fracture zone micrograph of selected sample from 1st run. (b) Magnification of the same sample exhibiting microvoids and dimples.

In contrast, samples in the best condition (7th run, which reported the best performance in the tensile test, achieving the highest UTS result) exhibited different fracture mechanisms. The fracture was predominantly ductile, as indicated by the white arrows highlighting the presence of dimples and micro-cracks, which are characteristic of ductile fracture, as depicted in Figure 11a. Furthermore, Figure 11b, captured at 300 \times magnification, illustrates the presence of dimples and microvoids, reinforcing the observation that the specimen exhibits good ductility [8]. The rest of the samples, including the as-received materials, exhibit similar fracture behavior, demonstrating consistent ductile fracture characteristics across these conditions.

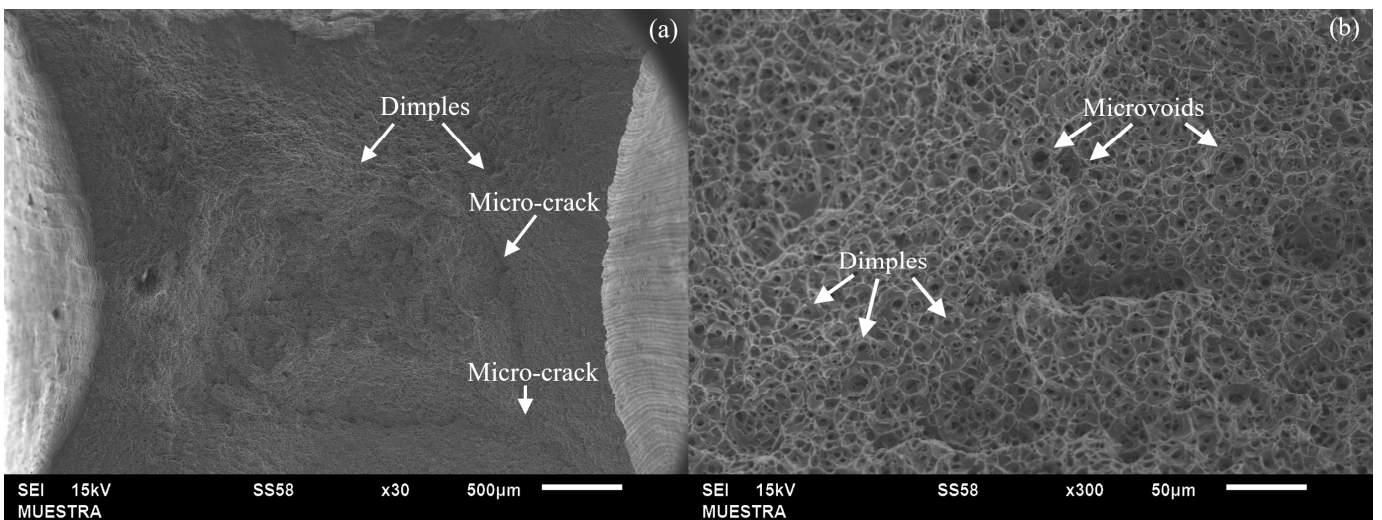


Figure 11. (a) Fracture zone micrograph of selected sample from 7th run. (b) Magnification of the same sample exhibiting microvoids and dimples.

The existence of distributed microvoids throughout the fractured aluminum matrix indicates good ductility and a favorable distribution of the strengthening β phase (Mg_2Si). The formation of microvoids occurs due to various mechanisms, including grain boundary sliding and dislocation movement [16]. During tensile deformation, stress concentrations can lead to the nucleation and growth of microvoids, which subsequently coalesce and form larger voids. These voids are then observed as dimples on the fracture surface. The localized coalescence of microvoids into larger dimples results from the interaction between

the plastic deformation mechanisms and the material microstructure. Grain boundaries, as well as dislocations, play a crucial role in this process. The sliding of grain boundaries and the movement of dislocations promote stress concentration around certain regions, leading to the nucleation and growth of microvoids. As deformation continues, these microvoids coalesce and form dimples, which are energy-absorbing features during the fracture process. A significant note is that fractographs obtained from tensile testing are more likely to reflect the plastic deformation ability of the material, corresponding to its elongation property, rather than solely indicating its strength. It is essential to consider that numerous factors, including the phases present within the material, influence the stress experienced by the material during testing.

4. Discussion

The mechanical testing results obtained through the DOE analysis (Section 3.1) start from the essence of the Taguchi DOE, which is the ability to construct an efficient and informative experimental design. By selecting fewer factors and levels, we aimed to simplify the experimental process and focus on the most influential variables while maintaining statistical robustness (as the ANOVA exhibited in Section 3.2). This approach allows us to achieve reliable results with fewer experiments than traditional full factorial designs, making the Taguchi DOE a valuable tool for experimental optimization. This approach is inherent to the Taguchi DOE's capabilities and aligns with the principles of sound experimental design. To analyze the results of evaluating the selected parameters on the ultimate tensile strength, we analyzed the hardness (Section 3.3) and the microstructure (Section 3.4); also, we conducted a hardening phase study (Section 3.5) and performed a fracture evaluation (Section 3.6).

Yield strength is relevant in mechanical testing evaluation, especially when the material's response to plastic deformation is predominant. However, we focus on UTS from the specific nature of processes such as welding and similar procedures, where the tensile strength often determines the final response due to several factors, including the variability in the 0.2% yield strength resulting from the mixture of microstructures generated during the cooling process. This variability can significantly impact the material's performance, particularly its ability to withstand applied stresses and resist deformation. In welding, the capacity of joints to withstand stress emphasizes the importance of considering the ultimate tensile strength in evaluating weldability and joint integrity [27]. Furthermore, in applications such as wear-resistance assessments, where hardness measurements serve as an initial indicator, ultimate tensile strength plays a crucial role, as it is directly correlated with hardness. Similarly, in phase transformation processes, the material's tensile strength is a key indicator of its response to heat-treatment, which is a critical consideration in various industries.

The Taguchi design of experiment is a potent and efficient methodology distinctively adept at discerning crucial factors, minimizing variability, enhancing performance, and conserving resources [18]. Particularly in assessing mechanical properties such as tensile strength, its application transcends traditional testing and measurement approaches (often performed as a trial-and-error procedure), offering a proficient and cost-effective means of optimization. Moreover, this methodology is evaluated using ANOVA to propose a prediction model that explains the contribution of each variable in the heat-treatment process to the final UTS value.

After ANOVA was applied to the Taguchi DOE, we obtained a regression model where the ultimate tensile strength of the alloy was linearly related to four factors: solutionizing temperature, aging temperature, solutionizing time, and aging time. It is important to note that the variable "aging temperature" was the least influential factor according to the analysis of variance, referring specifically to its relationship with the model and its generalization capability. This does not imply that aging temperature does not influence the outcome of the heat-treatment process because aging temperature is crucial in determining the final tensile strength.

Comparing the determination coefficient, the regression model obtained $R^2 = 93.18\%$. Thus, the model accounts for about 93% of the variability in the tensile strength response. Note that for the multiple regression model for the tensile strength data, $R_{adj}^2 = 91.95\%$. Therefore, we would conclude that adding the variable of aging temperature to the model does result in a meaningful reduction in unexplained variability in the response.

A cross-validation approach was employed to assess how well the model can predict results in different datasets. The $R_{prediction}^2$ was reserved for assessing the model's predictive ability. The obtained fitting results ($R_{prediction}^2$) was 89.75%, indicating that the model can explain approximately 90% of the variability observed in the test data for prediction and to evaluate the model's predictive capacity.

Therefore, at this point, it is crucial to explain the combined role of the variables involved in the heat-treatment process and the resulting ultimate tensile strength values in terms of the specific characteristics of this alloy. Increasing the solutionizing temperature to 540 °C allows more alloying elements, such as Mg, Si, and Cu, to remain in a solid solution [10,45]. Subsequently, these elements precipitate during artificial aging at high temperatures to form the Mg_2Si (β) phase [3,17]. In a study on various 6XXX-type alloys, Mrówka-Nowotnik and J. Sieniawski [36] determined that tensile strength in such alloys is influenced by the amount of Mg and Si present in a supersaturated solution, with Mg_2Si being the primary strengthening phase.

The reinforcement of the tensile strength of the alloy after the heat-treatment process can also be attributed to the movement of dislocations due to the presence of foreign particles from any other phase. However, if the temperature increases, as observed in run 7, with aging at 170 °C and a solutionizing temperature of 540 °C, when we relate hardness to tensile strength, samples treated at 530 °C exhibited lower hardness. This is reflected in decreased tensile strength or strengthening due to the coalescence of precipitates within a larger particle. Additionally, the annealing of defects occurs, which causes a reduction in obstacles to the movement of dislocations.

Ternary systems like Al-Mg-Si and alloys without an excess of Si exhibit a well-established precipitation sequence, as was demonstrated in previous studies using transmission electron microscopy (TEM) [37,46]:

- Solid solution
- GP (Guinier–Preston) zones
- Needle-shaped precipitates aligned with the (100) direction of the matrix and coherent with the Al matrix along their major axes
- β' phase (rod-shaped precipitates, semi-coherent with the matrix)
- β phase (Mg_2Si , plate-shaped equilibrium precipitates)

This sequence illustrates the compositional changes during precipitation, contributing to understanding the alloy's mechanical properties. It is worth noting that numerous studies in the literature have effectively utilized TEM to explain the microstructural evolution during aging treatments. Notably, research compiled by Ding [5] has provided comprehensive insights into the transformation sequence, including observing GP zones and the evolution of the beta phase through applying TEM. Additionally, references such as those by Jacobs [11], Saito [6], and Matsuda [47] have extensively investigated the phenomenon of beta dissolution utilizing TEM techniques, further supporting the efficacy of TEM in studying microstructural evolution during aging treatments. These findings align with the precipitation sequence previously reported [6,15]: super-saturated solid solution (SSSS) \rightarrow Si/Mg clusters \rightarrow Guinier-Preston (GP) zones \rightarrow β'' \rightarrow β' \rightarrow β .

Despite recrystallization (during the solutionizing stage), the β phase is still evident in the alloy after the thermal treatment, as we observed by XRD examination. The β phase is known for its strengthening effect on aluminum alloys, as it precipitates from the supersaturated solid solution during aging. The indexation of the diffraction peak at (220) confirms the existence of the β phase in the alloy (see Figure 9). It is worth noting that the morphology of β can vary, and in this alloy, it appears to exhibit plate-like or needle-like

shapes (see Figure 5). These precipitates contribute to the overall strengthening mechanism by impeding dislocation movement and enhancing the alloy's resistance to deformation. Thus, XRD analysis confirmed the microstructural changes that occur during the thermal treatment of the alloy. It also confirms the recrystallization of the aluminum matrix and the persistence of the strengthening β phase, being important in understanding the alloy's microstructural evolution and optimizing its mechanical properties.

Finally, the presence of dimples and microvoids on the fracture surface is desirable because it implies that the material has undergone plastic deformation before failure. This indicates that the alloy possesses good ductility and can withstand significant strains without sudden brittle failure. The favorable distribution of the β phase within the aluminum matrix further enhances the mechanical properties, contributing to the material's ability to deform plastically and absorb energy during fracture. This highlights its favorable mechanical behavior and ability to withstand deformation under tensile loading conditions.

5. Conclusions

This study focused on evaluating the heat-treatment parameters of the 6061 aluminum alloy to enhance its mechanical properties. The effects of solutionizing and aging temperatures on the Ultimate Tensile Strength were investigated systematically using the Taguchi design of experiment (DOE) method. The following key findings and conclusions were drawn from the study:

1. The mechanical testing results demonstrated a major influence of the solutionizing and aging parameters on the alloy's Ultimate Tensile Strength. The samples processed at a solutionizing temperature of 540 °C for 3 h, followed by aging at 170 °C for 18 h, exhibited the highest tensile strength (UTS = 293.7 MPa), while the samples processed at the lowest levels of these parameters showed the lowest tensile strength (UTS = 193.7 MPa).
2. The analysis of variance (ANOVA) revealed that aging temperature is the least influential factor affecting the Ultimate Tensile Strength. This factor has no statistically significant impact on the alloy's mechanical properties. However, it is essential for the final precipitation of the hardening phases and an important parameter in the heat-treatment process.
3. The microstructural analysis of the heat-treated samples confirmed the formation of equiaxed grains, strengthening precipitates, precipitate clusters, and β precipitates alongside Fe-Al-Si dispersoids. Energy-dispersive spectroscopy analysis also ratified the presence of elements precursors of the β phase (Al-Mg-Si) and dispersoid-forming elements (Al-Fe-Si).
4. X-ray diffraction analysis confirmed the presence of the β phase (Mg_2Si) in the alloy, both in the as-received and heat-treated samples. The persistence of the β phase after the heat-treatment indicated its contribution to the improved mechanical properties.
5. Fracture analysis revealed a ductile fracture mechanism in the alloy. The examination of the fractured samples supported the findings of enhanced tensile properties resulting from the systematic evaluation of heat-treatment parameters from the Taguchi DOE and ANOVA assessment.

The Taguchi DOE approach was successfully applied in this study to evaluate the heat-treatment parameters of the 6061-aluminum alloy by the analysis of variance. The results highlighted the significant impact of solutionizing and aging temperatures on the tensile strength, with the samples processed at higher levels of these parameters exhibiting superior mechanical properties. The microstructural and fracture analyses provided information about the mechanisms responsible for the improved properties, including the formation of strengthening precipitates and the persistence of the β phase. These findings contribute to the understanding and potential of enhancing the mechanical performance of the 6061-aluminum alloy in materials engineering applications and heat-treatment process optimization.

Author Contributions: Conceptualization, I.G.-F. and E.E.G.-G.; methodology, R.J.P.-A., C.E.C.-G. and J.C.D.-G.; software, C.E.C.-G. and R.J.P.-A.; validation, I.G.-F., R.J.P.-A., D.I.M.-D. and C.E.C.-G.; formal analysis, I.G.-F., H.M.H.-G., D.I.M.-D. and R.J.P.-A.; investigation, I.G.-F., C.E.C.-G. and L.F.-G.; resources, I.G.-F., J.C.D.-G. and H.M.H.-G.; writing—original draft preparation, I.G.-F., R.J.P.-A. and L.F.-G.; writing—review and editing, E.E.G.-G.; visualization, J.C.D.-G., E.E.G.-G. and I.G.-F. All authors have read and agreed to the published version of the manuscript.

Funding: This research received no external funding.

Data Availability Statement: The original contributions presented in the study are included in the article, further inquiries can be directed to the corresponding author.

Conflicts of Interest: Author H. M. Hernández-García was employed by the company InnovaBienes-tar de México, S.A.P.I. de C.V. The remaining authors declare that the research was conducted in the absence of any commercial or financial relationships that could be construed as a potential conflict of interest.

References

- Hirsch, J.; Al-Samman, T. Superior Light Metals by Texture Engineering: Optimized Aluminum and Magnesium Alloys for Automotive Applications. *Acta Mater.* **2013**, *61*, 818–843. [[CrossRef](#)]
- Polmear, I.J. *Light Alloys: From Traditional Alloys to Nanocrystals*, 4th ed.; Butterworth-Heinemann: Oxford, UK; Elsevier: Burlington, MA, USA, 2006; ISBN 978-0-7506-6371-7.
- Prillhofer, R.; Rank, G.; Berneder, J.; Antrekowitsch, H.; Uggowitzner, P.; Pogatscher, S. Property Criteria for Automotive Al-Mg-Si Sheet Alloys. *Materials* **2014**, *7*, 5047–5068. [[CrossRef](#)] [[PubMed](#)]
- Ostermann, F. *Anwendungstechnologie Aluminium*; Springer: Berlin/Heidelberg, Germany, 2014; ISBN 978-3-662-43806-0.
- Ding, L.; Jia, Z.; Nie, J.-F.; Weng, Y.; Cao, L.; Chen, H.; Wu, X.; Liu, Q. The Structural and Compositional Evolution of Precipitates in Al-Mg-Si-Cu Alloy. *Acta Mater.* **2018**, *145*, 437–450. [[CrossRef](#)]
- Saito, T.; Marioara, C.D.; Andersen, S.J.; Lefebvre, W.; Holmestad, R. Aberration-Corrected HAADF-STEM Investigations of Precipitate Structures in Al-Mg-Si Alloys with Low Cu Additions. *Philos. Mag.* **2014**, *94*, 520–531. [[CrossRef](#)]
- Van Huis, M.A.; Chen, J.H.; Sluiter, M.H.F.; Zandbergen, H.W. Phase Stability and Structural Features of Matrix-Embedded Hardening Precipitates in Al-Mg-Si Alloys in the Early Stages of Evolution. *Acta Mater.* **2007**, *55*, 2183–2199. [[CrossRef](#)]
- Naronikar, A.H.; Jamadagni, H.N.A.; Simha, A.; Saikiran, B. Optimizing the Heat Treatment Parameters of Al-6061 Required for Better Formability. *Mater. Today Proc.* **2018**, *5*, 24240–24247. [[CrossRef](#)]
- Subba Rao, E.; Ramanaiah, N. Influence of Heat Treatment on Mechanical and Corrosion Properties of Aluminium Metal Matrix Composites (AA 6061 Reinforced with MoS₂). *Mater. Today Proc.* **2017**, *4*, 11270–11278. [[CrossRef](#)]
- Aydi, L.; Khlif, M.; Bradai, C.; Spigarelli, S.; Cabibbo, M.; Mehtedi, M.E. Mechanical Properties and Microstructure of Primary and Secondary AA6063 Aluminum Alloy after Extrusion and T5 Heat Treatment. *Mater. Today Proc.* **2015**, *2*, 4890–4897. [[CrossRef](#)]
- Jacobs, M.H. The Structure of the Metastable Precipitates Formed during Ageing of an Al-Mg-Si Alloy. *Philos. Mag.* **1972**, *26*, 1–13. [[CrossRef](#)]
- Safyari, M.; Moshtaghi, M.; Hojo, T.; Akiyama, E. Mechanisms of Hydrogen Embrittlement in High-Strength Aluminum Alloys Containing Coherent or Incoherent Dispersoids. *Corros. Sci.* **2022**, *194*, 109895. [[CrossRef](#)]
- Safyari, M.; Moshtaghi, M.; Kuramoto, S. Environmental Hydrogen Embrittlement Associated with Decohesion and Void Formation at Soluble Coarse Particles in a Cold-Rolled Al-Cu Based Alloy. *Mater. Sci. Eng. A* **2021**, *799*, 139850. [[CrossRef](#)]
- Guzmán, I.; Granda, E.; Cruz, C.; Martínez, D.; Vargas, B.; Acevedo, J.; Cruz, G.; Avila, Y.; Velazquez, R.; Flores, L. Corrosion Performance and Mechanical Strength in Aluminum 6061 Joints by Pulsed Gas Metal Arc Welding. *Materials* **2022**, *15*, 6226. [[CrossRef](#)] [[PubMed](#)]
- Zhang, X.Z.; Chen, T.J.; Chen, Y.S.; Wang, Y.J.; Qin, H. Effects of Solution Treatment on Microstructure and Mechanical Properties of Powder Thixoforming 6061 Aluminum Alloy. *Mater. Sci. Eng. A* **2016**, *662*, 214–226. [[CrossRef](#)]
- Zhang, S.; Chen, T.; Cheng, F.; Li, P. A Comparative Characterization of the Microstructures and Tensile Properties of As-Cast and Thixoforged in Situ AM60B-10 Vol% Mg₂Sip Composite and Thixoforged AM60B. *Metals* **2015**, *5*, 457–470. [[CrossRef](#)]
- Chen, T.J.; Wang, W.; Zhang, D.H.; Ma, Y.; Hao, Y. Effects of Heat Treatment on Microstructure and Mechanical Properties of ZW21 Magnesium Alloy. *J. Alloys Compd.* **2013**, *546*, 28–40. [[CrossRef](#)]
- Roy, R.K. *Design of Experiments Using the Taguchi Approach: 16 Steps to Product and Process Improvement*; Wiley: New York, NY, USA, 2001; ISBN 978-0-471-36101-5.
- Leisk, G.; Saigal, A. Taguchi Analysis of Heat Treatment Variables on the Mechanical Behavior of Alumina/Aluminum Metal Matrix Composites. *Compos. Eng.* **1995**, *5*, 129–142. [[CrossRef](#)]
- Yang, J.; Ni, Y.; Li, H.; Fang, X.; Lu, B. Heat Treatment Optimization of 2219 Aluminum Alloy Fabricated by Wire-Arc Additive Manufacturing. *Coatings* **2023**, *13*, 610. [[CrossRef](#)]
- Afrasiabi, H.A.; Khayati, G.R.; Ehteshamzadeh, M. Studying of Heat Treatment Influence on Corrosion Behavior of AA6061-T6 by Taguchi Method. *Int. J. Eng.* **2014**, *27*, 1423–1430. [[CrossRef](#)]

22. Alphonse, M.; Bupesh Raja, V.K.; Vivek, M.S.; Sai Deepak Raj, N.V.; Satya Sai Darshan, M.; Bharmal, P. Effect of Heat Treatment on Mechanical Properties of Forged Aluminium Alloy AA2219. *Mater. Today Proc.* **2021**, *44*, 3811–3815. [[CrossRef](#)]
23. Montgomery, D.C.; Peck, E.A.; Vining, G.G. *Introduction to Linear Regression Analysis*, 5th ed.; Wiley Series in Probability and Statistics; Wiley: Hoboken, NJ, USA, 2012; ISBN 978-0-470-54281-1.
24. Arai, T.; Baker, G.M.; Bates, C.E.; Becherer, B.A.; Bell, T.; Bird, E.L.; Bramfitt, B.L.; Brennan, R.L.; Brooks, C.R.; Brown, T.D.; et al. *ASM Handbook: Volume 4: Heat Treating*; 9. print; ASM International: Materials Park, OH, USA, 2009; ISBN 978-0-87170-379-8.
25. Manente, A.; Timelli, G. Optimizing the Heat Treatment Process of Cast Aluminium Alloys. In *Recent Trends in Processing and Degradation of Aluminium Alloys*; Ahmad, Z., Ed.; InTech: London, UK, 2011; ISBN 978-953-307-734-5.
26. Montgomery, D.C. *Design and Analysis of Experiments*, 8th ed.; John Wiley & Sons, Inc.: Hoboken, NJ, USA, 2013; ISBN 978-1-118-14692-7.
27. AWS D1. 2/D1.2M *Structural Welding Code—Aluminum*; American Welding Society: Miami, FL, USA, 2013; pp. 83–87.
28. Guzmán, I.; Granda, E.; Acevedo, J.; Martínez, A.; Dávila, Y.; Velázquez, R. Comparative in Mechanical Behavior of 6061 Aluminum Alloy Welded by Pulsed GMAW with Different Filler Metals and Heat Treatments. *Materials* **2019**, *12*, 4157. [[CrossRef](#)] [[PubMed](#)]
29. Guzmán, I.; Granda, E.; Vargas, B.; Cruz, C.; Avila, Y.; Acevedo, J. Tensile and Fracture Behavior in 6061-T6 and 6061-T4 Aluminum Alloys Welded by Pulsed Metal Transfer GMAW. *Int. J. Adv. Manuf. Technol.* **2019**, *103*, 2553–2562. [[CrossRef](#)]
30. ASTM International. ASTM E8/E8M—16a Standard Test Methods for Tension Testing of Metallic Materials. In *ASTM Volume 03.01 Metals—Mechanical Testing; Elevated and Low-Temperature Tests; Metallography*; ASTM International: Washington, DC, USA, 2016; Volume 03.01.
31. ASTM International. ASTM E3-11 (2017) Standard Guide for Preparation of Metallographic Specimens. In *ASTM Volume 03.01 Metals—Mechanical Testing; Elevated and Low-Temperature Tests; Metallography*; ASTM International: Washington, DC, USA, 2017; Volume 03.01.
32. ASTM International. ASTM B209—Specification for Aluminum and Aluminum-Alloy Sheet and Plate. In *Specification for Aluminum and Aluminum-Alloy*; ASTM International: Washington, DC, USA, 2021; Volume 02.02.
33. Doncaster, C.P.; Davey, A.J.H. *Analysis of Variance and Covariance: How to Choose and Construct Models for the Life Sciences*; Cambridge University Press: Cambridge, UK, 2007; ISBN 978-0-521-86562-3.
34. Korner-Nievergelt, F.; Roth, T.; Von Felten, S.; Guélat, J.; Almasi, B.; Korner-Nievergelt, P. Normal Linear Models. In *Bayesian Data Analysis in Ecology Using Linear Models with R, BUGS, and STAN*; Elsevier: Amsterdam, The Netherlands, 2015; pp. 33–68; ISBN 978-0-12-801370-0.
35. Mrówka-Nowotnik, G. Influence of Chemical Composition Variation and Heat Treatment on Microstructure and Mechanical Properties of 6xxx Alloys. *Arch. Mater. Sci. Eng.* **2010**, *46*, 98–107.
36. Mrówka-Nowotnik, G.; Sieniawski, J. Influence of Heat Treatment on the Microstructure and Mechanical Properties of 6005 and 6082 Aluminium Alloys. *J. Mater. Process. Technol.* **2005**, *162–163*, 367–372. [[CrossRef](#)]
37. Edwards, G.A.; Stiller, K.; Dunlop, G.L.; Couper, M.J. The Precipitation Sequence in Al–Mg–Si Alloys. *Acta Mater.* **1998**, *46*, 3893–3904. [[CrossRef](#)]
38. Marioara, C.D.; Andersen, S.J.; Jansen, J.; Zandbergen, H.W. The Influence of Temperature and Storage Time at RT on Nucleation of the β'' Phase in a 6082 Al–Mg–Si Alloy. *Acta Mater.* **2003**, *51*, 789–796. [[CrossRef](#)]
39. Yassar, R.S.; Field, D.P.; Weiland, H. Transmission Electron Microscopy and Differential Scanning Calorimetry Studies on the Precipitation Sequence in an Al–Mg–Si Alloy: AA6022. *J. Mater. Res.* **2005**, *20*, 2705–2711. [[CrossRef](#)]
40. Demir, H.; Gündüz, S. The Effects of Aging on Machinability of 6061 Aluminium Alloy. *Mater. Des.* **2009**, *30*, 1480–1483. [[CrossRef](#)]
41. Sanamar, S.; Brokmeier, H.-G.; Schell, N. Formation of the Intermetallic Phases $Al_{12}Mg_{17}$ and Al_3Mg_2 during Heating of Elemental Al–Mg Composites Studied by High-Energy X-ray Diffraction. *J. Alloys Compd.* **2022**, *911*, 165114. [[CrossRef](#)]
42. Rao, P.N.; Singh, D.; Brokmeier, H.-G.; Jayaganthan, R. Effect of Ageing on Tensile Behavior of Ultrafine Grained Al 6061 Alloy. *Mater. Sci. Eng. A* **2015**, *641*, 391–401. [[CrossRef](#)]
43. Jogi, B.F.; Brahmankar, P.K.; Nanda, V.S.; Prasad, R.C. Some Studies on Fatigue Crack Growth Rate of Aluminum Alloy 6061. *J. Mater. Process. Technol.* **2008**, *201*, 380–384. [[CrossRef](#)]
44. Zhang, L.; Zhong, H.; Li, S.; Zhao, H.; Chen, J.; Qi, L. Microstructure, Mechanical Properties and Fatigue Crack Growth Behavior of Friction Stir Welded Joint of 6061-T6 Aluminum Alloy. *Int. J. Fatigue* **2020**, *135*, 105556. [[CrossRef](#)]
45. Tan, C.; Said, M.R.; Chen, W. The Tensile Strength Effects on Precipitation Heat Treatment of 6061-T6 Aluminum Alloy. In *Volume 3: ASME/IEEE 2009 International Conference on Mechatronic and Embedded Systems and Applications; 20th Reliability, Stress Analysis, and Failure Prevention Conference*; ASMEDC: San Diego, CA, USA, 2009; pp. 839–845.
46. Murayama, M.; Hono, K.; Miao, W.F.; Laughlin, D.E. The Effect of Cu Additions on the Precipitation Kinetics in an Al–Mg–Si Alloy with Excess Si. *Metall. Mater. Trans. A* **2001**, *32*, 239–246. [[CrossRef](#)]
47. Matsuda, K.; Sakaguchi, Y.; Miyata, Y.; Uetani, Y.; Sato, T.; Kamio, A.; Ikeno, S. Precipitation Sequence of Various Kinds of Metastable Phases in Al-1.0mass% Mg₂Si-0.4mass% Si Alloy. *J. Mater. Sci.* **2000**, *35*, 179–189. [[CrossRef](#)]

Disclaimer/Publisher’s Note: The statements, opinions and data contained in all publications are solely those of the individual author(s) and contributor(s) and not of MDPI and/or the editor(s). MDPI and/or the editor(s) disclaim responsibility for any injury to people or property resulting from any ideas, methods, instructions or products referred to in the content.